

# Nanoscale

Accepted Manuscript



This is an *Accepted Manuscript*, which has been through the Royal Society of Chemistry peer review process and has been accepted for publication.

*Accepted Manuscripts* are published online shortly after acceptance, before technical editing, formatting and proof reading. Using this free service, authors can make their results available to the community, in citable form, before we publish the edited article. We will replace this *Accepted Manuscript* with the edited and formatted *Advance Article* as soon as it is available.

You can find more information about *Accepted Manuscripts* in the [Information for Authors](#).

Please note that technical editing may introduce minor changes to the text and/or graphics, which may alter content. The journal's standard [Terms & Conditions](#) and the [Ethical guidelines](#) still apply. In no event shall the Royal Society of Chemistry be held responsible for any errors or omissions in this *Accepted Manuscript* or any consequences arising from the use of any information it contains.

# Conduction Control at Ferroic Domain Walls via External Stimuli

J. C. Yang<sup>1\*</sup>, C. H. Yeh<sup>2\*</sup>, Y. T. Chen<sup>3</sup>, S. C. Liao<sup>4</sup>, R. Huang<sup>5</sup>, H. J. Liu<sup>1,3</sup>, C. C. Hung<sup>6</sup>,  
S. H. Chen<sup>6</sup>, S. L. Wu<sup>2</sup>, C. H. Lai<sup>4</sup>, Y. P. Chiu<sup>3</sup>, P. W. Chiu<sup>2</sup> and Y. H. Chu<sup>1</sup>

<sup>1</sup> Department of Materials Science and Engineering, National Chiao Tung University,  
Hsinchu, 300, Taiwan

<sup>2</sup> Institute of Electronics Engineering, National Tsing Hua University, HsinChu, 300, Taiwan

<sup>3</sup> Department of Physics, National Sun Yat-sen University, Kaohsiung 80424, Taiwan

<sup>4</sup> Department of Materials Science and Engineering, National Tsing Hua University, Hsinchu,  
300, Taiwan

<sup>5</sup> Key Laboratory of Polar Materials and Devices, Ministry of Education, East China Normal  
University, Shanghai 200062, China

<sup>6</sup> ThinTech Materials Technology Co., Ltd., Kaohsiung, 82151, Taiwan

**\* These authors contributed equally in this work.**

**Corresponding Author: Prof. Ying-Hao Chu**

**Email: [yhc@nctu.edu.tw](mailto:yhc@nctu.edu.tw)**

**Address: Room 709, Engineering Building VI, 1001 University Road, Hsinchu,  
30010, Taiwan**

**Phone: +1-510-501-9307**

## Abstract

The intriguing functionalities at nano-sized domain walls have recently spawned a new paradigm for developing novel nanoelectronics due to the versatile characteristics. In this study, we explore new scenario to modulate local conduction of ferroic domain walls. Three controlling parameters, external electrical field, magnetic field and light, are introduced to the 90° domain walls (90° DWs) of BiFeO<sub>3</sub>. The electrical modulation is realized by means of electrical transport, where the mobility of 90° DWs can be altered by gating voltage. We further use the ferromagnetic/antiferromagnetic coupling to reveal the inherent magnetism at the DWs. With the established magnetic nature, magnetotransport has been conducted to introduce the magnetic controlling parameter, where a giant positive magnetoresistance change can be observed up to 200%. In addition, light modulated conduction, a very core factor toward to multifunctional applications, is successfully demonstrated (current enhancement by a factor of 2 with 11W white lamp). These results offer new insights to discover the tunability of domain wall nanoelectronics.

## Keywords:

domain walls, multiferroic, BiFeO<sub>3</sub>, nanoelectronics, multifunctional interfaces

## Introduction

A great demand for small electronic devices with multifunctionalities has arisen in pursuit of fast information computation and communication. For numerous functional materials that are being proposed and explored, complex oxide interfaces have emerged as one of the most exciting systems due to their unique properties, and offer new possibilities for next-generation electronic devices<sup>[1-3]</sup>. Recently, three types of complex oxide interfaces have been established<sup>[4]</sup>, namely, the heterointerfaces, tubular interfaces and homointerfaces.

Intriguing electronic transport behaviors have been discovered in these interfaces, including a highly mobile quasi-two dimensional electron gas formed between two insulators<sup>[3,5]</sup>; the local conduction found at the tubular interfaces of BiFeO<sub>3</sub>-CoFe<sub>2</sub>O<sub>4</sub> (BFO-CFO) heterostructure<sup>[4]</sup> and domain walls (DWs) in ferro/multiferroics<sup>[6-8]</sup>. Therefore, in the push for practical applications, it is desirable to gain further control of the interface functionalities through external stimuli. The modulation of the local conduction at heterointerface (LaAlO<sub>3</sub>/SrTiO<sub>3</sub>)<sup>[9-11]</sup> and the BFO-CFO tubular interface were demonstrated recently<sup>[12]</sup>. However, the external control of domain wall (complex oxide homointerface) conduction is yet to be fully explored. Multiferroic BFO provides robust coupling between electricity and magnetism, and the potential to manipulate one through the other<sup>[13-14]</sup>. The domain walls of BFO have suggested new possibilities to explore the interplays of magnetic and electronic characteristics at an interface<sup>[15-16]</sup>. In light of both scientific research and practical applications<sup>[17]</sup>, BFO DWs serve as potential candidates of the multifunctional electronic devices for next generation.

In this study, we take 90° DWs in BFO as a model homointerface to demonstrate the conduction of domain walls can be modulated by external electric field, magnetic field, and light, as illustrated in **Figure 1(a)**. Epitaxial BFO thin films were prepared on NdScO<sub>3</sub>(110) (NSO) substrate by pulsed laser deposition at 700 °C in the oxygen pressure of 100 mTorr and cooled in 1 atm after deposition. The particular role of a tensile strain has been used to stabilize the orthorhombic phase, in which the depolarization field suppresses the <111><sub>pc</sub> polarizations of BFO parent phase to <110><sub>pc</sub> directions<sup>[18]</sup>. The boundaries of two adjacent domains with <110><sub>pc</sub> polarizations give rise to the 90° DWs in BFO. However, in order to build up a model 90° DWs platform, we applied proper anisotropic strain provided by orthorhombic NSO substrate to exclude two of the possible structure variants and thus resulted in periodic 90° DWs.

## Results and discussion

The key features of periodic  $90^\circ$  DWs are distinguished by a combination of piezoresponce force microscopy (PFM) and x-ray diffraction. The topography and ferroelectric domain patterns of  $90^\circ$  DWs are imaged by atomic force microscope and PFM, as shown in **Figure 1(b)**. The long-range elastic interaction and structural nature give rise to the topography in polar materials. A lateral lamellar morphology is discovered in  $90^\circ$  DW BFO, in which the elastic relaxation and lattice structure lead to the surface reconstruction, resulting in the planar topography<sup>[18]</sup>. Three strong contrasts (bright, dark and brown) in the in-plane (IP) PFM image with scanning tip cantilever along  $[100]_{pc}$  direction together with negligible response of the out-of-plane (OOP) PFM image were observed. These PFM results confirmed the  $\langle 110 \rangle_{pc}$  polarization of the BFO/NSO sample, which is the fundamental building unit to construct the periodic  $90^\circ$  DWs in BFO. Furthermore, the PFM results have unveiled the periodic feature of  $90^\circ$  domain patterns with  $\{001\}_{pc}$  domain boundaries.

X-ray diffraction serves as an ideal tool to reveal the periodicity of the patterns. Thorough  $q_x$  -scans are executed with the x-ray parallel to  $[001]_o/[100]_{pc}$  direction. Constant spacing in the  $q_x$ -scans from  $(001)_{pc}$  to  $(004)_{pc}$  are observed as shown in **Figure 1(c)**. In  $q_x$ -scans, tilting of the crystal structure of BFO gives rise to the increasing splitting from  $(001)_{pc}$  to  $(004)_{pc}$  scans, whereas the reflections of periodic planar domain result in the constant splitting in  $q_x$ -scans. In  $90^\circ$  DWs BFO, the planar domains formed by orthorhombic BFO phase result in the constant spacing in the  $q_x$ -scans from  $(001)_{pc}$  to  $(004)_{pc}$ . As a result, the domain spacing could be extracted by Williamson-Hall plot<sup>[19]</sup>, in which the interception of the Williamson-Hall plot (not shown here) give rise to a 15 nm periodic satellite reflection of the periodic domain patterns, as marked in **Figure 1(a)**. Such a result is consistent with the value extracted from PFM study. It is the periodic domain patterns that enable us to build up a model system to facilitate the experimental setup and to quantize the conduction characteristics.

The well-aligned domain architectures were directly imaged via a spherical aberration corrected scanning transmission electron microscope (Cs-corrected STEM). A typical high angle annular dark-field (HAADF) STEM image obtained from the cross-section sample is shown in **Figure 2(a)**. It reveals that the interface between the BFO thin film and the NSO substrate is atomically flat and the lattices match to each other perfectly. No mismatch dislocations and other defects can be observed. The Fe ions shifted to the middle-left in the Bi rectangles in the BFO thin film, indicating that the polarization direction is along the  $\langle 110 \rangle_{pc}$ . Two  $90^\circ$  DWs with discernable lattice distortion were imaged, as labeled in between two red dotted lines in **Figure 2(a)**.

To explore the local electronic environment at the domain walls, we use scanning tunneling microscopy (STM) to unveil the electronic structure across the  $90^\circ$  DWs. In the present STM measurements, the sample was cleaved in the STM chamber *in situ* to obtain the cross-sectional slice of the domain patterns as shown schematically in **Figure 2(b)**. All STM experiments reported here were performed in an UHV chamber with base pressure of approximately  $5 \times 10^{-11}$  Torr. Our STM and scanning tunneling spectroscopy (STS) studies provide direct experimental indication into the nature and origin of the electronic conductivity at  $90^\circ$  DWs in BFO. The local electronic density of states (DOS) at each site was determined from the first derivative of the tunneling current with respect to the sample bias ( $dI/dV$ ). The electronic image in **Figure 2(b)** recorded the spatial dependence of the tunneling current at -2.1 V in the vicinity of the domain wall in BFO. The variations of the tunneling current characteristics reveal distinct electronic properties across the domain wall, involving a decrease in the local band gap and built-in asymmetric potential barriers at domain walls. Analyzed layer-by-layer  $dI/dV$  curves can clearly address the characteristics of the electrostatic potential steps across the domain wall. In **Figure 2(c)**, with the characteristics of  $dI/dV$  curves, the atomic-scale evolution of local electronic property across the domain wall can be quantitatively depicted and directly traced. The visualized atomic-scale band alignment

provides a direct observation of how the band structures evolve across the domain wall. The key feature is that the change of band gap is attributed from the shift of the current onset at the both positive and negative sample bias. The obvious downward shift in the conduction-band edge and upward shift in the valence-band edge can be correlated with the Fe-O octahedral deformations and the surroundings of O 2p-Fe 3d states in the wall region<sup>[16]</sup>. The finding of a significant reduction of the electronic bandgap suggests the promising conduction scenario of the 90° DWs, a new type of multiferroic domain wall in BFO.

In order to explore the electrical control on the conduction of 90° DWs, we have fabricated the three-terminal test architecture shown in **Figure 3(a)**. In this test structure, transport measurements as functions of temperature, magnetic field, and gate voltage have been carried out. Three types of device configurations, as shown in the cartoons in **Figure 3(b)**, were prepared for the study on the conduction of the 90° domain walls: As shown in **Figure 3(b)**, electrical conduction is only observable in devices with electrodes aligned perpendicular to the domain walls (Device A and B). The device with longer electrodes (Device A) is connected to more domain walls and hence shows higher conduction. The absence of electrical conduction in Device C as well as the higher conduction of Device A clearly indicates that it is domain walls that give rise to the charge conduction. We further study the electric-field gating effects on the domain wall conduction using three-terminal devices with top-gate geometry (as illustrated by the cartoon in **Figure 3(a)**). One should note that the application of gate voltage did not alter the direction of ferroelectric polarization of the domains underneath the gate electrode because no bottom electrode is used. The domain walls remained intact throughout the measurements. As shown in **Figure 3(c)**, results of the field-effect transport at room temperature show significant increases of conduction at domain walls when applying positive gate bias, revealing n-type conduction at the 90° DWs. The observed n-type conduction and activation energy found on temperature dependent experiments (see supplementary material) have suggested the electron chemical doping

resulted from the oxygen vacancies at and/or surrounding the domain walls, which are in nice agreement with previous studies<sup>[8,15]</sup>. As a result, the observed enhanced conduction can be understood by an electronic conduction mechanism, driven by a local change in the bandgap as consequences of the discontinuity in in-plane polarizations and the local defect chemistry. Further information buildup with the top-gate geometry yields carrier mobility values of  $\sim 1.6$ - $1.8 \text{ cm}^2/\text{V}\cdot\text{s}$  at a source-drain electric field of  $8 \text{ kV/cm}$ , and with a gate voltage dependence, as shown in **Figure 3(d)**. To get access to practical applications for high-density information communication and low-energy consumption, one can significantly enhance the carrier density via divalent-ion doping<sup>[20]</sup>, where the advanced modification of the domain wall conductivity will be revealed elsewhere. These results have clearly elucidated the ability for tuning the carrier transport via external electrical fields.

To fulfil the magnetic modulation, a detailed understanding of the magnetic state of  $90^\circ$  DWs is required since the conduction of the BFO domain walls was predicted to be highly correlated between the free carriers, electronic structures, and the local spin states at the walls<sup>[16]</sup>. The magnetic anisotropy of  $90^\circ$  DWs is probed by the ferromagnetic-antiferromagnetic exchange coupling with Permalloy ( $\text{Ni}_{81}\text{Fe}_{19}$ , Py) layer. We deposited 5nm-thick Py layer on BFO under a magnetic field of  $120 \text{ Oe}$  along  $[1-10]_o/[010]_{pc}$  and  $[001]_o/[100]_{pc}$  directions, respectively, and the corresponding magnetic hysteresis loops are shown in **Figure 4(a)** and **4(b)**. For the samples with deposition field along  $[1-10]_o/[010]_{pc}$  direction, i.e. along the DWs, a typical exchange-biased loop<sup>[21]</sup> with bias field ( $H_{cb}$ ) of  $10 \text{ Oe}$  is observed when measuring along the deposition field; whereas a hard-axis loop with anisotropy field ( $H_k$ ) of  $50 \text{ Oe}$  is obtained when measuring along directions that are perpendicular to the deposition field. A similar phenomenon has been revealed in previous study<sup>[22]</sup>. These results indicate that the coupling between BFO and Py creates an easy axis and a bias field, which are parallel to the deposition field direction. For sample with deposition field along  $[001]_o/[100]_{pc}$ , however, shows abnormal and interesting behaviors: the

loop measured along  $[001]_o/[100]_{pc}$  showed the a  $H_{eb}$  of 13 Oe and a shape of hard-axis loop with  $H_k$  of 50 Oe. On the other hand, loop measured along  $[1-10]_o/[010]_{pc}$  showed a double-shifted feature, two easy-axis loops with opposite  $H_{ex}$  of 13 Oe. Based on those findings, we may conclude that the deposition field along  $[001]_o/[100]_{pc}$  direction would create a bias field that lies at  $[001]_o/[100]_{pc}$  and an easy axis lies along  $[1-10]_o/[010]_{pc}$ . In other words, exchange coupling between Py and  $90^\circ$  DWs BFO would always create an easy axis parallel to  $[1-10]_o/[010]_{pc}$  regardless the direction of the deposition field. This phenomenon is attributed to the intrinsic anisotropy of uncompensated spins in  $90^\circ$  DWs BFO. The other indication based on this observation is the fact of the collinear coupling between the uncompensated spins and the spin of Py, owing to the fact that the perpendicular coupling would not create exchange bias in the similar systems<sup>[23]</sup>. When it comes to the deposition field applied along  $[001]_o/[100]_{pc}$ , a part of uncompensated spins rotates to the  $[001]_o/[100]_{pc}$  and forms the exchange bias along  $[001]_o/[100]_{pc}$ , whereas the other part of spins do not rotate and form the easy axis along  $[1-10]_o/[010]_{pc}$ . Most of uncompensated spins in BFO pin the spins of Py at  $[001]_o/[100]_{pc}$  axis and only certain part of uncompensated spins rotate and couple collinearly with spins in Py within this feature, which gives rise to the bias field that is parallel to the deposition field. Despite exchange coupling mechanism is unclear yet, it is believed that the magnetic spins at the walls are highly correlated to the strain states and direction of adjacent ferroelectric dipoles<sup>[15,22]</sup>. Such results have indicated the hints to control the local conduction with external magnetic stimulation.

The entangled multiferroic orders of BFO thin films enable us to integrate the magnetic and electronic control parameters. To achieve so, high-field magnetotransport of the  $90^\circ$  DWs is studied with the charge transport with in-plane magnetic field parallel to the domain walls, as illustrated in **Figure 4(c)**. An innovative and remarkable scenario builds on an observation of the magnetoresistance, which is, noteworthy, non-trivially high (above 200% at 8 T) and positive magnetoresistance. A scenario based on multilayer magnetic coupling is proposed to

explain the positive magnetoresistance. Assuming that the canted spin at the domain wall forms ferromagnetic clusters, whose polarization is aligned to the external magnetic field, the conduction through these ferromagnetic clusters (i.e. the magnetoresistance) depends on the coupling between the clusters, resulting in either negative magnetoresistance, when ferromagnetically coupled, or positive magnetoresistance, when anti-ferromagnetically coupled. This scenario is similar to the proposed model for the positive giant magnetoresistance effect observed in multilayer devices<sup>[24-25]</sup>. The observed large positive magnetoresistance implies the anti-ferromagnetic coupling in canted spin cluster at the 90° domain walls, if this scenario applies. However, more studies are required and are being undertaken for explaining the details about the transport mechanism behind the non-trivial magnetoresistance.

In addition to magnetic and electric tuning factors, we have explored light as an additional route to create multi-conduction states in the device. An 11 W white lamp with continuous wavelength has been used as the light source. Remarkably, the conduction current doubles as light is shone on the device, as shown in **Figure 4(d)**. The well-aligned domain patterns create a built-in potential across the domain walls, which give rise to an enhanced charge separation and a higher photovoltaic voltage<sup>[26]</sup>. The photo-response is related to the band gap of BFO thin film and the local band gap drop across the domain walls. More free carriers are excited under the exposure to the light, the charge separation has then achieved by the local ferroelectric polarizations, resulting in the increased conduction level. Furthermore, the sensitive responses along with light irradiation suggested a higher photo current when constructing a photovoltaic device. We have demonstrated the experiment to introduce the photonic controlling parameter for modulating the local conductivity of the homointerfaces. Furthermore, it is remarkable that the DW width is only merely ~2 nm according to our previous study<sup>[27]</sup>, indicating the promising size feature of the potential applications. The finding has once again lighted up the variable tuning factors when designing the

functionalities of such homointerfaces

## Conclusions

In summary, we have demonstrated the modulation of local conduction of  $90^\circ$  DWs in BFO thin film via external stimuli, namely electronic, magnetic as well as light tuning factors. X-ray diffraction, piezoresponse force microscopy and transmission electron microscope have provided the general features of the  $90^\circ$  DWs. Scanning tunneling microscopy has indicated a change of local band gap at the walls, which served as the conduction origin of the domain walls. We examined the magnetic structure in  $90^\circ$  DW through ferromagnetic/antiferromagnetic exchange coupling. Spin flop and uncompensated spin across the walls are highly correlated to the local ferroelectric polarization, which suggest a promising magnetic modulation of the local conduction. Magnetotransport has been conducted to integrate the magnetic and electronic parameters, where a giant positive magnetoresistance change is observed when applying an external field parallel to the current and the  $90^\circ$  DWs. We also provide a promising feature to include photo-response as additional controlling factor, the sensitive and increased conduction change suggesting a new route for pursuing new photovoltaic device and multiple digit computation. Our results have offered a new perspective to control the local conduction in ferroic domain walls with various stimuli, which shed the light on constructing multi-functionalities and potential applications of nano-sized homointerfaces.

## Experimental Section

*Sample fabrication:* Epitaxial BiFeO<sub>3</sub> thin films were fabricated on (110) oriented NdScO<sub>3</sub> (NSO) single crystal substrate via pulsed laser deposition (PLD) with a KrF ( $\lambda=248$  nm) excimer laser. Pulsed laser beam was focused on BiFeO<sub>x</sub> ceramic target with an energy density of 3J/cm<sup>2</sup> and repetition rate of 10Hz. Samples were deposited at the substrate temperature of 700 °C and with 100 mTorr oxygen pressure. Samples were cooled to room temperature in an oxygen pressure of 1 atm. The ferromagnetic/antiferromagnetic bilayer samples were prepared by depositing 5-nm thick Ni<sub>81</sub>Fe<sub>19</sub> with 5-nm Ta capping layer on BFO layer. Both two layers are deposited by magnetron sputtering with based pressure of 5x10<sup>-8</sup> Torr at room temperature. A magnetic field of 120 Oe was applied during the deposition to set the direction of exchange coupling.

*Characterization of structure and physical properties:* Surface morphology (AFM) and piezoresponse force microscopy (PFM) were performed using Bruker Multimode VIII. High-resolution X-ray diffraction techniques were taken to examine the crystal quality and domain spacing of BiFeO<sub>3</sub> (BFO) thin films at beamline BL17A in the National Synchrotron Radiation Research Center (NSRRC), Taiwan. The BFO heterostructure was characterized by a Cs-corrected HAADF-STEM (STEM; JEOL JEM2100F, Cs-corrector; CEOS GmbH). In the present scanning tunnelling microscopy (STM) measurements, the sample was cleaved in the STM chamber *in-situ* to obtain the cross-sectional slice of the BFO heterostructure. STM experiments were performed in an ultra-high-vacuum (UHV) chamber with base pressure of approximately 5×10<sup>-11</sup> Torr. STM and STS images were simultaneously acquired at temperature of 100 K. Transport behaviors of BFO domain walls were measured in manner of three-terminal architecture with source, drain and gate electrodes. All electrodes were made of gold and bonded with copper wires for standard electrical measurements. The measurements of magnetic hysteresis loops were performed at room temperature by using MicroMag vibrating sample magnetometer (VSM) 3900 (Princeton Measurements

Cooperation). Magneto-transport measurements were operated at 4K via quantum design physical property measurement system (PPMS) using a standard four-probe method.

### Acknowledgements

This work was supported by the National Science Council of Republic of China (under contract No. NSC-101-2119-M-009-003-MY2), Ministry of Education (grant No. MOE-ATU 101W961), and Center for Interdisciplinary Science at National Chiao Tung University. Prof. R. Huang is supported by Shanghai Pujiang talents plan (Grant No. 11PJ1402900). Dr. C. C. Hung and Dr. S. H. Chen acknowledge the financial support of Southern Taiwan Science Park under contract No. 102CC01. We would like to thank Dr. R. K. Vasudevan for his help in manuscript discussion. Jan-Chi Yang and Chao-Hui Yeh contributed equally to this work.

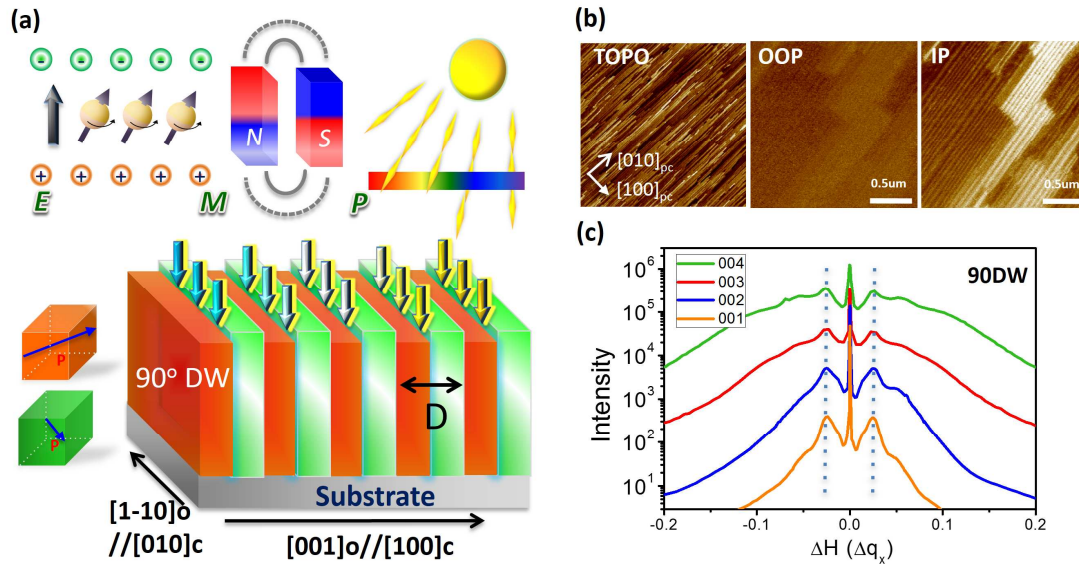
### Notes and references

- [1] J. Mannhart, D. G. Schlom, *Science* 2010, 327, 1607.
- [2] Y. Tokunaga, N. Furukawa, H. Sakai, Y. Taguchi, T. Arima, Y. Tokura, *Nature Mater.* 2009, 8, 558.
- [3] A. Ohtomo, H. Y. Hwang, *Nature* 2003, 427, 423.
- [4] Y. H. Hsieh, J. M. Liou, B. C. Huang, C. W. Liang, Q. He, Q. Zhan, Y. P. Chiu, Y. C. Chen, Y. H. Chu, *Adv. Mater.* 2012, 24, 4564.
- [5] N. Reyren, S. Thiel, A. D. Caviglia, L. F. Kourkoutis, G. Hammerl, C. Richter, C. W. Schneider, T. Kopp, A. -S. Rüetschi, D. Jaccard, M. Gabay, D. A. Muller, J. -M. Triscone, J. Mannhart, *Science* 2007, 317, 1196.
- [6] J. Seidel, L. W. Martin, Q. He, Q. Zhan, Y. -H. Chu, A. Rother, M. E. Hawkrigde, P. Maksymovych, P. Yu, M. Gajek, N. Balke, S. V. Kalinin, S. Gemming, F. Wang, G. Catalan, J. F. Scott, N. A. Spaldin, J. Orenstein, R. Ramesh, *Nature Mater.* 2009, 8, 229.
- [7] S. Farokhipoor, B. Noheda, *Phys. Rev. Lett* 2012, 107, 127601.

- [8] J. Seidel, P. Maksymovych, Y. Batra, A. Katan, S. -Y. Yang, Q. He, A. P. Baddorf, S. V. Kalinin, C. -H. Yang, J. -C. Yang, Y. -H. Chu, E. K. H. Salje, H. Wormeester, M. Salmeron, R. Ramesh *Phys. Rev. Lett* 2010, 105, 197603.
- [9] S. Thiel, G. Hammerl, A. Schmehl, C. W. Schneider, J. Mannhart, *Science* 2006, 313, 1942.
- [10] A. D. Caviglia, S. Gariglio, N. Reyren, D. Jaccard, T. Schneider, M. Gabay, S. Thiel, G. Hammerl, J. Mannhart, J. -M Triscone, *Nature* 2008, 456, 624.
- [11] A. Brinkman; M. Huijben, M. Van Zalk, J. Huijben, U. Zeitler, J. C. Maan, W. G. Van Der Wiel, G. Rijnders, D. H. A. Blank, H. Hilgenkamp, *Nature Mater.* 2007, 6, 493.
- [12] Y. H. Hsieh, E. Strelcov, J. M. Liou, C. Y. Shen, Y. C. Chen, S. V. Kalinin, Y. H. Chu, *ACS Nano* 2013, 7, 8627.
- [13] T. Zhao, A. Scholl, F. Zavaliche, K. Lee, M. Barry, A. Doran, M. P. Cruz, Y. H. Chu, C. Ederer, N. A. Spaldin, R. R. Das, D. M. Kim, S. H. Baek, C. B. Eom, R. Ramesh, *Nature Mater.* 2006, 5, 823.
- [14] Y. -H. Chu, L. M. Martin, M. B. Holcomb, M. Gajek, S. J. Han, Q. He, N. Balke, C. H. Yang, D. Lee, W. Hu, Q. Zhan, P. L. Yang, A. Fraile-Rodriguez, A. Scholl, S. X. Wang, R. Ramesh, *Nature Mater.* 2008, 7, 478.
- [15] Q. He, C. H. Yeh, J. C. Yang, G. Singh-Bhalla, C. W. Laing, P. W. Chiu, G. Catalan, L. W. Martin, Y. H. Chu, J. F. Scott, R. Ramesh, *Phys. Rev. Lett* 2012, 108, 067203.
- [16] A. Lubk, S. Gemming, N. A. Spaldin, *Phys. Rev. B* 2009, 80, 104110.
- [17] G. Catalan, J. Seidel, R. Ramesh, J. F. Scott, *Rev. of Mod. Phys.* 2012, 84, 119.
- [18] J. C. Yang, Q. He, S. J. Suresha, C. Y. Kuo, C. Y. Peng, R. C. Haislmaier, M. A. Motyka, G. Sheng, C. Adamo, H. J. Lin, Z. Hu, L. Chang, L. H. Tjeng, E. Arenholz, N. J. Podraza, M. Bernhagen, R. Uecker, D. G. Schlom, V. Gopalan, L. Q. Chen, C. T. Chen, R. Ramesh, Y. H. Chu, *Phys. Rev. Lett.* 2012, 109, 247606.
- [19] G. K. Williamson, W. H. Hall, *Acta Meta.* 1953, 1, 22.

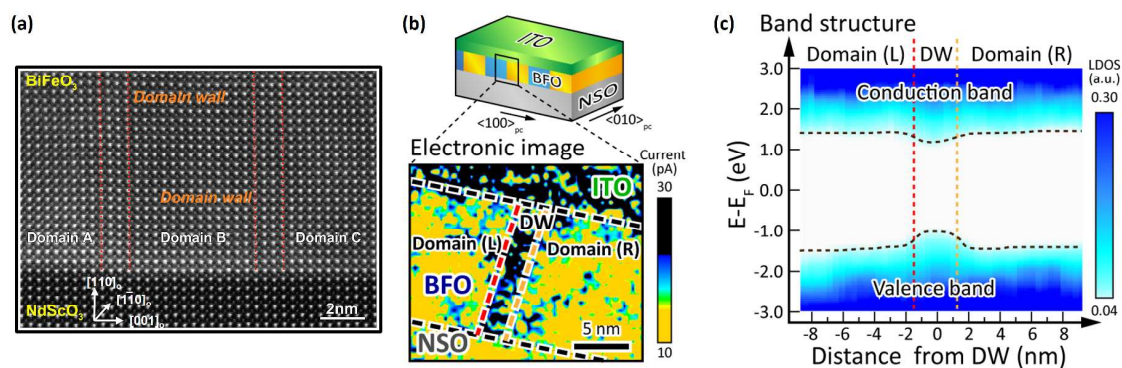
- [20] K. Brinkman, T. Iijima, H. Takamura, *Japan. J. Appl. Phys.* 2007, 46, L93.
- [21] J. Nogue's, I. K. J. Schuller, *Magn. Magn. Mater.* 1999, 192, 203.
- [22] L. W. Martin, Y. H. Chu, M. B. Holcomb, M. Huijben, P. Yu, S. J. Han, D. Lee, S. X. Wang, R. Ramesh *Nano Lett.* 2008, 8, 2050.
- [23] T. C. Schulthess, W. H. Butler, *Phys. Rev. Lett* 1998, 81, 4516.
- [24] R. Mallik, E. V. Sampathkumaran, P. L. Paulose, *Appl. Phy. Lett.* 1997, 71, 2385.
- [25] S. S. P. Parkin, *Appl. Phy. Lett.* 1987, 63, 1987.
- [26] S. Y. Yang, J. Seidel, S. J. Byrnes, P. Shafer, C. H. Yang, M. D. Rossell, P. Yu, Y. H. Chu, J. F. Scott, J. W. Ager III, L. M. Martin, R. Ramesh, *Nature Nanotechnol.* 2010, 5, 143.
- [27] Y. P. Chiu, Y. T. Chen, B. C. Huang, M. C. Shih, J. C. Yang, Q. He, C. W. Liang, J. Seidel, Y. C. Chen, R. Ramesh, Y. H. Chu, *Adv. Mater.* 2011, 23, 1530.

Figure 1



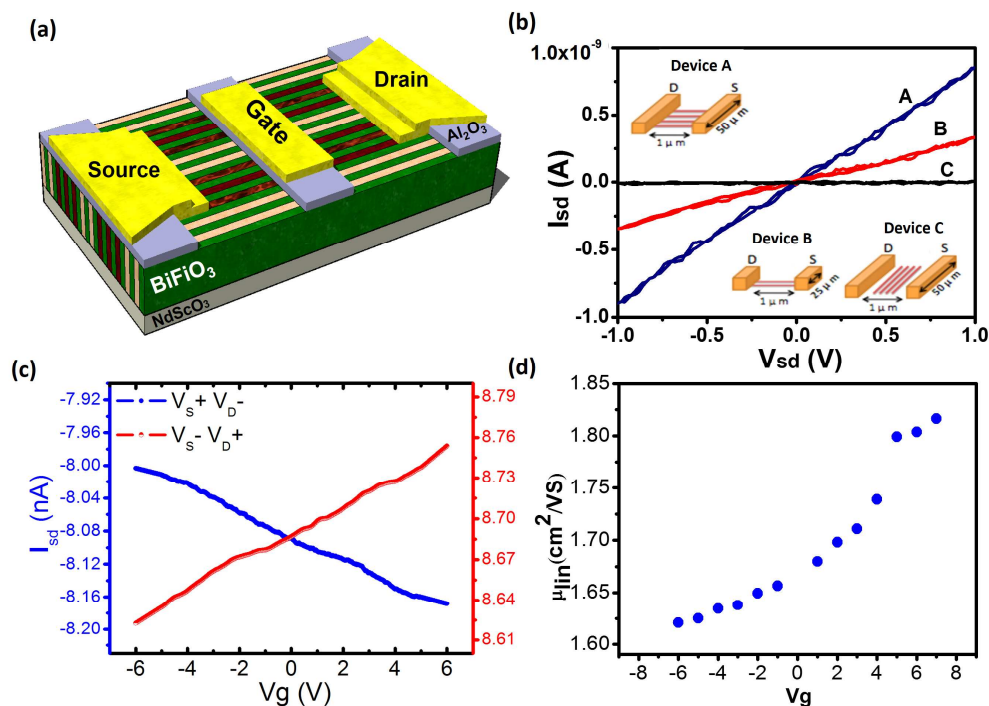
**Figure 1.** (a) Schematic toward to the modulation the local conduction of the 90° domain walls in BiFeO<sub>3</sub> via electrical, magnetic as well as photonic tuning factors. The orange and green patterns represent the BiFeO<sub>3</sub> domains with respect to different polarizations, where a homointerface, domain wall, emerges at the boundary of the two distinct domains. (b) The topography, in-plane and out-of-plane piezoforce response microscopy images of 90° DW sample. The images were probed with the scanning cantilever along with [100]<sub>pc</sub> direction (c) High-resolution x-ray H-scans of 90° DW thin films.

Figure 2



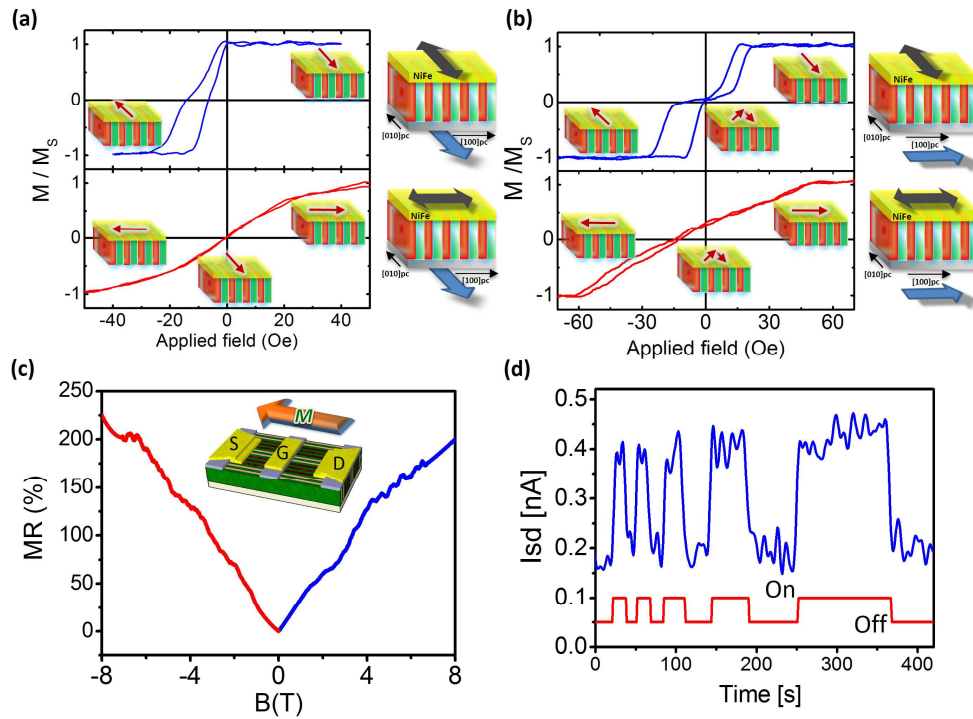
**Figure 2.** (a) HAADF STEM image of  $90^\circ$  domain walls in  $\text{BiFeO}_3/\text{NdScO}_3$  thin film in cross-section view, where the location of the domain walls are labeled in between two red dotted lines. (b) The experimental architecture of the  $90^\circ$  domain wall sample for cross-sectional scanning tunneling microscopy (upper side) and the spatial dependence of the tunneling current at  $-2.1$  V in the vicinity of the domain wall in BFO (downward side). The ITO protection layer has been deposited as scanning buffer and the location reference. (c) The band structure constructed by the first derivative of the tunneling current with respect to the sample bias ( $dI/dV$ ) in the electronic mapping scan.

Figure 3



**Figure 3.** (a) Experimental configuration of three-terminal  $90^\circ$  domain wall devices with top-gate geometry. (b) The current-voltage curves with respect to three types of device configurations. Devices A with  $50\text{-}\mu\text{m}$ -long source-drain electrodes that are aligned perpendicular to the domain walls, devices B with  $25\text{-}\mu\text{m}$ -long source-drain electrodes that are aligned perpendicular to the domain walls, and devices C with  $50\text{-}\mu\text{m}$ -long source-drain electrodes that are aligned parallel to the domain walls. (c) The gating effects of the  $90^\circ$  domain walls. The blue and red curves represent for the measurements with identical yet reverse electrical potentials of  $V_{sd} = 8\text{ V}$  and  $V_{sd} = -8\text{ V}$ , respectively. (d) Carrier mobility as a function of gate voltages extrapolated at an electric field of  $8\text{ kV/cm}$  across the source and drain electrodes.

Figure 4



**Figure 4.** (a)(b) Exchange coupling study of 90° domain walls and ferromagnetic Permalloy (Ni<sub>81</sub>Fe<sub>19</sub>, Py) top layers. 5nm-thick Py layers were deposited on BiFeO<sub>3</sub> with applied magnetic field of 120 Oe along [1-10]<sub>o</sub>/[010]<sub>pc</sub> and [001]<sub>o</sub>/[100]<sub>pc</sub> directions, respectively. The M-H loops are measured parallel and perpendicular to the deposited fields, as illustrated in the cartoons. (c) Magnetotransport measurement as a function of magnetic field. The magnetic field is applied parallel to the electron transport direction. (d) The photonic response of 90° domain walls. On-off states of the photo pulses are depicted in the red curve while the blue curve shows the current variation along with photo pulses.

## TOC

**Multiple conduction controls of ferroic domain walls** via external stimuli are demonstrated for the sake of new nanoelectronics. The conduction level of  $90^\circ$  domain walls in multiferroic  $\text{BiFeO}_3$  can be elegantly tuned by electric, magnetic fields and light, enabling such nano-sized homointerface to be promising candidates for next generation multifunctional devices.

Keyword:

domain walls, multiferroic,  $\text{BiFeO}_3$ , nanoelectronics, multifunctional materials

*Jan-Chi Yang, Chao-Hui. Yeh, Yu-Ting Chen, Sheng-Chieh Liao, Rong Huang, Heng-Jui Liu, Chien-Chi Hung, Shih-Hsun Chen, Shan-Lin Wu, Chih-Huang Lai, Ya-Ping Chiu, Po-Wen Chiu and Ying-Hao Chu\**

**Conduction Control at Ferroic Domain Walls via External Stimuli**